



Originally published as:

Lu, B., Luo, Z., Zhong, B., Zhou, H., Flechtner, F., Förste, C., Barthelmes, F., Zhou, R. (2018): The gravity field model IGGT_R1 based on the second invariant of the GOCE gravitational gradient tensor. - *Journal of Geodesy*, 92, 5, pp. 561—572.

DOI: <http://doi.org/10.1007/s00190-017-1089-8>

1 **The gravity field model IGGT_R1 based on the**
2 **second invariant of the GOCE gravitational gradient**
3 **tensor**

4 **Biao Lu · Zhicai Luo · Bo Zhong · Hao**
5 **Zhou · Frank Flechtner · Christoph**
6 **Förste · Franz Barthelmes · Rui Zhou**

7
8 Received: date / Accepted: date

Biao Lu
School of Geodesy and Geomatics, Wuhan University, 430072 Wuhan, PR China.
GFZ German Research Centre for Geosciences, Telegrafenberg, 14473 Potsdam, Germany.
Department of Geodesy and Geoinformation Science, Technical University of Berlin, 10623
Berlin, Germany.
E-mail: biaolu@gfz-potsdam.de

Zhicai Luo
MOE Key Laboratory of Fundamental Physical Quantities Measurement, School of Physics,
Huazhong University of Science and Technology, 430074 Wuhan, PR China.
Institute of Geophysics, Huazhong University of Science and Technology, 430074 Wuhan,
PR China.
E-mail: zcluo@hust.edu.cn

Bo Zhong
School of Geodesy and Geomatics, Wuhan University, 430072 Wuhan, PR China.
Key Laboratory of Geospace Environment and Geodesy, Ministry of Education, Wuhan
University, 430079 Wuhan, PR China.
E-mail: bzhong@sgg.whu.edu.cn

Hao Zhou
MOE Key Laboratory of Fundamental Physical Quantities Measurement, School of Physics,
Huazhong University of Science and Technology, 430074 Wuhan, PR China.
E-mail: zhouh@hust.edu.cn

Frank Flechtner
GFZ German Research Centre for Geosciences, Telegrafenberg, 14473 Potsdam, Germany.
Department of Geodesy and Geoinformation Science, Technical University of Berlin, 10623
Berlin, Germany.
E-mail: flechtne@gfz-potsdam.de

Christoph Förste
GFZ German Research Centre for Geosciences, Telegrafenberg, 14473 Potsdam, Germany.
E-mail: foer@gfz-potsdam.de

Franz Barthelmes
GFZ German Research Centre for Geosciences, Telegrafenberg, 14473 Potsdam, Germany.
E-mail: bar@gfz-potsdam.de

Rui Zhou

Abstract Based on tensor theory, three Invariants of the Gravitational Gradient Tensor (IGGT) are independent of the Gradiometer Reference Frame (GRF). Compared to traditional methods for calculation of gravity field models based on the Gravity field and steady-state Ocean Circulation Explorer (GOCE) data, which are affected by errors in the attitude indicator, using IGGT and least squares method avoids the problem of inaccurate rotation matrices. The IGGT approach as studied in this paper is a quadratic function of the gravity field model's spherical harmonic coefficients. The linearized observation equations for the least squares method is obtained using a Taylor expansion, and the weighting equation is derived using the law of error propagation. We also investigate the linearization errors using existing gravity field models and find that this error can be ignored since the used a-priori model EIGEN-5C is sufficiently accurate. One problem when using this approach is that it needs all six independent Gravitational Gradients (GGs), but the components V_{xy} and V_{yz} of GOCE are worse due to the non-sensitive axes of the GOCE gradiometer. Therefore we use synthetic GGs for both inaccurate gravitational gradient components derived from the a-priori gravity field model EIGEN-5C. Another problem is that the GOCE GGs are measured in a band-limited manner. Therefore, a forward and backward finite impulse response band-pass filter is applied to the data, which can also eliminate filter caused phase change. The Spherical Cap Regularization Approach (SCRA) and the Kaula rule are then applied to solve the polar gap problem caused by GOCE's inclination of 96.7° . With the techniques described above, a degree/order 240 gravity field model called IGGT_R1 is computed. Since the synthetic components of V_{xy} and V_{yz} are not band-pass filtered, the signals outside the measurement bandwidth are replaced by the a-priori model EIGEN-5C. Therefore this model is practically a combined gravity field model which contains GOCE GGs signals and long wavelength signals from the a-priori model EIGEN-5C. Finally, IGGT_R1's accuracy is evaluated by comparison with other gravity field models in terms of difference degree amplitudes, the geostrophic velocity in the Agulhas current area, gravity anomaly differences as well as by comparison to GNSS/Leveling data.

Keywords Invariants of the gravitational gradient tensor · Least squares method · Linearization · Band-pass filter · GOCE

Abbreviations

CHAMP Challenging Minisatellite Payload
 DIR_R1 GO_CONS_GCF_2_DIR_R1
 DIR_R2 GO_CONS_GCF_2_DIR_R2
 ERF Earth-fixed Reference Frame
 ESA European Space Agency

49	GGs Gravitational Gradients
50	GOCE Gravity field and steady-state Ocean Circulation Explorer
51	GRACE Gravity Recovery and Climate Experiment
52	GRF Gradiometer Reference Frame
53	ICGEM International Centre for Global Earth Models
54	IGGT Invariants of the Gravitational Gradient Tensor
55	IRF Inertial Reference Frame
56	LNOF Local North Oriented Frame
57	MDT Mean Dynamic Topography
58	MPI Message Passing Interface
59	OpenMP Open Multi-Processing
60	RLE Relative Linearization Error
61	SCRA Spherical Cap Regularization Approach
62	SDs Spectral Densities
63	SPW_R1 GO_CONS_GCF_2_SPW_R1
64	TIM_R1 GO_CONS_GCF_2_TIM_R1

65 1 Introduction

66 The Gravity field and steady-state Ocean Circulation Explorer (GOCE) differs
67 from previous Earth gravity satellite missions, e.g., Challenging Minisatellite
68 Payload (CHAMP) and Gravity Recovery and Climate Experiment (GRACE)
69 as it can provide the much more detailed measurements of the GGs of Earth's
70 gravity field. Calculation of gravity field models based on these measured GGs
71 has become a very important research domain and several methods for deter-
72 mination of gravity field models from GGs have been developed. The three
73 main methods are the space-wise approach, the time-wise approach and the
74 direct approach (Rummel and Colombo, 1985; Rummel, 1993; Klees et al,
75 2000; Pail and Plank, 2002; Migliaccio et al, 2004; Bruinsma et al, 2010a;
76 Migliaccio et al, 2011; Pail et al, 2011; Yi, 2012; Bruinsma et al, 2014). The
77 European Space Agency (ESA) has already distributed several gravity models
78 constructed using these three methods through the International Centre for
79 Global Earth Models (ICGEM) (Barthelmes, 2009; Barthelmes and Förste,
80 2011). The space-wise approach is based on least squares collocation and takes
81 advantage of the spatial correlation of the gravitational field signal. The time-
82 wise approach is based on a least squares method, but takes advantage of the
83 time correlation of the gravitational field signal along the satellite's orbit. The
84 direct approach is also based on a least squares method and builds observa-
85 tion equations and normal equations directly from in-situ GOCE GGs. While
86 processing the GGs for these methods, errors may be introduced when using
87 the GOCE star tracker data to relate the azimuth of the GRF to other coord-
88 inate systems. Although the direct method uses GGs measured in the GRF
89 to build the normal equation, the coefficients of every observation equation
90 must be rotated from Earth Centered Earth Fixed coordinates to the GRF.
91 Thus the inaccuracies in the transformation matrix cannot be avoided. Specif-

ically, investigations by Pail and Plank (2002), Pail et al (2005) and Yu and Zhao (2010) found that 1 arcsec attitude errors can lead the data processing accuracy to barely reach a relative magnitude of $10^{-6} - 10^{-7}$.

In view of this challenging problem, Rummel and Colombo (1985) began to investigate how to use the IGGT to build gravity field models. Holota (1989) discussed how to use the theory of boundary value problems for partial differential equations in satellite gradiometry. Then Sacerdote and Sansò (1989) analyzed the effects of orbit and attitude errors on GGs, and they found that using a reference gravity field including the J_2 term is preferable. At the same time, Vermeer (1990) built up three independent invariants and studied how the difference method for GGs could reduce the effects of the satellite's attitude and rotation. They also analyzed the spectrum relationship between the differencing method's result and the gravitational signal. More recently, Baur et al (2008) expanded the invariant theory in detail from the invariant system and eigenspace. They parameterized the invariants and performed numerical simulations, but the parameterization in the spherical polar coordinate is complicated. Boundary value problems with a sphere approximation including a J_2 term are shown by (Yu and Zhao, 2010; Yu and Wan, 2013). Specifically, the gravity field models are built using spherical harmonic analysis according to the boundary value conditions. However, this requires gridding the GOCE gravitational gradient measurements and using spherical harmonic integral discretization which can introduce errors that are difficult to eliminate.

Based on these previous studies, we investigate how to use IGGT to directly determine gravity field models using a least squares method in this paper. We study the linearization of IGGT mathematically from the Taylor expansion. Furthermore, the Lagrange type reminder or linearization error is investigated by existing, high accurate gravity field models to prove that it can be ignored when a-priori accurate gravity field model is chosen, e.g. EIGEN-5C (Förste et al, 2008). So it doesn't need iteratively calculations used by Baur et al (2008) during numerical simulations to eliminate the linearization error which is time-consuming in the least squares method. As the non-uniform accuracy of GOCE GGs, the weighting formula of IGGT is derived by the law of error propagation. To deal with the inaccurate components V_{xy} and V_{yz} , we use synthetic GGs for both inaccurate gravitational gradient components derived from the a-priori gravity field model. As GOCE GGs are measured in a band-limited manner, filtering is necessary for different approaches. The Wiener filter along the orbit to reduce the highly time correlated noise of the gradiometer which is generally used for collocation procedure e.g. the space-wise approach (Reguzzoni and Tselfes, 2009). Autoregressive moving average filtering is applied to both the time-wise approach and the direct approach, but it is a kind of filtering of entire spectrum (full decorrelation) for the time-wise approach while filtering within the measurement bandwidth for the direct approach (Schuh, 2003; Pail et al, 2011). We also applied a band-pass filter as the direct approach to suppress the signal outside the measurement bandwidth. This makes the result largely independent of the variability in the colored noise. Furthermore we use a finite impulse response band-pass filter forward and backward to eliminate the filter

caused phase change and the signals outside the measurement bandwidth are replaced by the a-priori model. In this way, it avoids to filter both sides of the observations and the columns of the design matrix during calculations like the time-wise approach and the direct approach. This kind of filtering and replacement method can be used both for spherical harmonic analysis and direct least squares method according to Wan et al (2012). Therefore the final gravity field model built in this paper is practically a combined one which is improved by GOCE GGs signals from the a-priori gravity field model. This is also one reason why we replace the inaccurate components V_{xy} and V_{yz} by the a-priori gravity field model. To verify our approach we built a gravity field model called IGGT.R1 using GOCE GGs and we compared it with other relevant gravity field models and also evaluated it by using GNSS/Leveling data.

2 The Direct Calculation Model for IGGT

2.1 Tensor Invariants Method

According to the symmetric and trace-free characteristics of the gravitational gradient tensor, Γ , three invariants can be identified by:

$$\begin{cases} I_1 = \text{tr}(\Gamma) = 0 \\ I_2 = \frac{1}{2} \text{tr}(\Gamma)^2 = -\frac{1}{2}(V_{11}^2 + V_{22}^2 + V_{33}^2) - V_{12}^2 - V_{13}^2 - V_{23}^2 \\ I_3 = \det \Gamma = V_{11}V_{22}V_{33} + 2V_{12}V_{13}V_{23} - V_{11}V_{23}^2 - V_{22}V_{13}^2 - V_{33}V_{12}^2 \end{cases} \quad (1)$$

The first tensor invariant is the trace of the gravitational tensor and its application in geopotential recovery yields the trivial solution as shown by Baur et al (2008). The second tensor invariant comprises all 6 independent gravitational gradient tensor components. Furthermore it is a quadratic function of the spherical harmonic coefficients of the gravity field:

$$I_2 = I = -\frac{1}{2}(V_{xx}^2 + V_{yy}^2 + V_{zz}^2) - V_{xy}^2 - V_{xz}^2 - V_{yz}^2 \quad (2)$$

It has been shown in several theoretical studies (e.g. Baur et al, 2008; Rummel et al, 2011) that also the second as well as third invariant can be used to compute a global gravity model solution. Since the second invariant is easier to linearize than the third one, we focus on the second one here in this study.

2.2 Parameterization and Linearization

The expression of the gravitational potential in terms of spherical harmonic series is given by (e.g. Heiskanen and Moritz (1967)):

$$V(r, \vartheta, \lambda) = \frac{GM}{R} \sum_{n=0}^{N_{\max}} \left(\frac{R}{r}\right)^{n+1} \sum_{m=0}^n (\bar{C}_{nm} \cos m\lambda + \bar{S}_{nm} \sin m\lambda) \bar{P}_{nm}(\cos \vartheta) \quad (3)$$

167 where GM is the Geocentric gravitational constant, R is Earth equatorial
 168 radius. In the following the variable x represents the spherical harmonic coef-
 169 ficients as given in Eq.(4), the mathematical operator Sigma in Eq.(4) means
 170 the numbering scheme instead of the summation of elements as shown by
 171 Schuh (1996); the indexed gravity field model coefficients \bar{C}_{nm} and \bar{S}_{nm} are
 172 preferable for calculating the high degree normal equation (e.g. Colombo, 1981;
 173 Schuh, 1996).

$$x = \{\bar{C}_{nm}, \bar{S}_{nm}\} \Rightarrow \left\{ \sum_{n=2}^{n_{\max}} \bar{C}_{n0}, \sum_{m=1}^{n_{\max}} \left\{ \sum_{n=\max(2,m)}^{n_{\max}} \bar{C}_{nm}, \sum_{n=\max(2,m)}^{n_{\max}} \bar{S}_{nm} \right\} \right\} \quad (4)$$

174 As the tensor invariant I in the GRF is same as in the Local North Ori-
 175 ented Frame (LNOF), we use it in the GRF directly, but linearize it in the
 176 LNOF. The tensor invariant I is a second order function of the GGs in the
 177 LNOF, while the GGs in the LNOF are first order functions of the spherical
 178 harmonic coefficients. Thus I is a quadratic function of the spherical harmonic
 179 coefficients. A Taylor expansion (Taylor, 1717; Courant and John, 2012) of I
 180 with the Lagrange form of the remainder is applied to generate Eq.(5):

$$\begin{aligned} I(x) - I(x_0) &= \sum_{p=1}^{n=1} \frac{1}{p!} (\Delta x_1 \frac{\partial}{\partial x_1} + \cdots + \Delta x_m \frac{\partial}{\partial x_m})^p I(x)|_{x=x_0} \\ &+ \frac{1}{(n+1)!} (\Delta x_1 \frac{\partial}{\partial x_1} + \cdots + \Delta x_m \frac{\partial}{\partial x_m})^{n+1} \\ &I(x)|_{x=x_0+\theta h} \quad (0 < \theta < 1) \end{aligned} \quad (5)$$

181 where x_1, x_2, \dots, x_m is the spherical harmonic coefficients. The Taylor expan-
 182 sion of I exists since the first and second order partial derivatives of I with
 183 respect to x_i exist. Eq.(7) and Eq.(9) correspondingly yield the partial deriva-
 184 tives of I and the GGs with respect to x_i . In Eq.(5), n is equal to 1 as I
 185 contains only second order partial derivatives of x_i , h is set to $x - x_0$ and θ is
 186 some real number between 0 and 1. For x_0 we choose EIGEN-5C as the a-priori
 187 gravity field model as it is of a relatively high accuracy and doesn't contain
 188 GOCE data. Next we analyze the Lagrange remainder, or the linearization
 189 error, using the existing, high accurate gravity field model EGM2008 (Pavlis
 190 et al, 2012) and another high accurate and GOCE containing gravity field
 191 model EIGEN-6C4 (Förste et al, 2015a) to calculate $I(x)$. The linearization
 192 error is defined by Eq.(6):

$$\begin{aligned} \text{Error}_L &= I(x) - I(x_0) - \sum_{p=1}^{n=1} \frac{1}{p!} (\Delta x_1 \frac{\partial}{\partial x_1} + \cdots + \Delta x_m \frac{\partial}{\partial x_m})^p I(x)|_{x=x_0} \\ &= I(x) - I(x_0) - (\Delta x_1 \frac{\partial I(x)|_{x=x_0}}{\partial x_1} + \cdots + \Delta x_m \frac{\partial I(x)|_{x=x_0}}{\partial x_m}) \end{aligned} \quad (6)$$

193 As shown in Eq.(6), the derivatives of I with respect to x_i should be de-
 194 termined before analyzing the linearization error using existing gravity field

195 models. The purpose of the linearization is to determine the relationship be-
 196 tween the IGGT and the gravity field model geopotential coefficients. The
 197 derivative of I with respect to x_i is based on Eq.(2) and given by Eq.(7):

$$\begin{aligned} \frac{\partial I}{\partial x_i} = & -(V_{xx} \frac{\partial V_{xx}}{\partial x_i} + V_{yy} \frac{\partial V_{yy}}{\partial x_i} + V_{zz} \frac{\partial V_{zz}}{\partial x_i} + 2V_{xy} \frac{\partial V_{xy}}{\partial x_i} \\ & + 2V_{xz} \frac{\partial V_{xz}}{\partial x_i} + 2V_{yz} \frac{\partial V_{yz}}{\partial x_i}) \end{aligned} \quad (7)$$

198 The transformation relationship of GGs between earth center spherical
 199 coordinates and LNOF is given by Eq.(8) as shown by Koop (1993) and is
 200 used to get the GGs' derivatives in the LNOF to geopotential coefficients of
 201 the gravity field model.

$$\left\{ \begin{aligned} V_{zz} &= V_{rr} \\ V_{xx} &= \frac{1}{r} V_r + \frac{1}{r^2} V_{\vartheta\vartheta} \\ V_{yy} &= \frac{1}{r} V_r + \frac{1}{r^2 \tan \vartheta} V_{\vartheta} + \frac{1}{r^2 \sin^2 \vartheta} V_{\lambda\lambda} \\ V_{xy} &= \frac{1}{r^2 \sin^2 \vartheta} V_{\vartheta\lambda} - \frac{\cos \vartheta}{r^2 \sin^2 \vartheta} V_{\lambda} \\ V_{xz} &= \frac{1}{r^2} V_{\vartheta} - \frac{1}{r} V_{r\vartheta} \\ V_{yz} &= \frac{1}{r^2 \sin \vartheta} V_{\lambda} - \frac{1}{r \sin \vartheta} V_{r\lambda} \end{aligned} \right. \quad (8)$$

202 The corresponding derivatives of the GGs with respect to the spherical
 203 harmonic coefficients are given in Eq.(9). The coefficients of the observation

204 matrix are then obtained by substituting them into Eq.(7).

$$\left\{ \begin{array}{l}
 \frac{\partial V_{zz}}{\partial \bar{C}_{nm}} = \frac{GMR^n}{r^{n+3}}(n+1)(n+2)\bar{P}_{nm}(\cos \vartheta) \cos m\lambda \\
 \frac{\partial V_{xx}}{\partial \bar{C}_{nm}} = \frac{GMR^n}{r^{n+3}}(-(n+1)\bar{P}_{nm}(\cos \vartheta) + \frac{\partial^2 \bar{P}_{nm}(\cos \vartheta)}{\partial \vartheta^2}) \cos m\lambda \\
 \frac{\partial V_{yy}}{\partial \bar{C}_{nm}} = \frac{GMR^n}{r^{n+3}}(-(n+1)\bar{P}_{nm}(\cos \vartheta) + \frac{1}{\tan \vartheta} \frac{\partial \bar{P}_{nm}(\cos \vartheta)}{\partial \vartheta} \\
 \quad - \frac{m^2}{\sin^2 \vartheta} \bar{P}_{nm}(\cos \vartheta)) \cos m\lambda \\
 \frac{\partial V_{xy}}{\partial \bar{C}_{nm}} = \frac{GMR^n}{r^{n+3}}(-m \frac{1}{\sin \vartheta} \frac{\partial \bar{P}_{nm}(\cos \vartheta)}{\partial \vartheta} + m \frac{\cos \vartheta}{\sin^2 \vartheta} \bar{P}_{nm}(\cos \vartheta)) \sin m\lambda \\
 \frac{\partial V_{xz}}{\partial \bar{C}_{nm}} = \frac{GMR^n}{r^{n+3}}(n+2) \frac{\partial \bar{P}_{nm}(\cos \vartheta)}{\partial \vartheta} \cos m\lambda \\
 \frac{\partial V_{yz}}{\partial \bar{C}_{nm}} = \frac{GMR^n}{r^{n+3}} \frac{1}{\sin \vartheta} (-m(n+2)\bar{P}_{nm}(\cos \vartheta)) \sin m\lambda \\
 \frac{\partial V_{zz}}{\partial \bar{S}_{nm}} = \frac{GMR^n}{r^{n+3}}(n+1)(n+2)\bar{P}_{nm}(\cos \vartheta) \sin m\lambda \\
 \frac{\partial V_{xx}}{\partial \bar{S}_{nm}} = \frac{GMR^n}{r^{n+3}}(-(n+1)\bar{P}_{nm}(\cos \vartheta) + \frac{\partial^2 \bar{P}_{nm}(\cos \vartheta)}{\partial \vartheta^2}) \sin m\lambda \\
 \frac{\partial V_{yy}}{\partial \bar{S}_{nm}} = \frac{GMR^n}{r^{n+3}}(-(n+1)\bar{P}_{nm}(\cos \vartheta) + \frac{1}{\tan \vartheta} \frac{\partial \bar{P}_{nm}(\cos \vartheta)}{\partial \vartheta} \\
 \quad - \frac{m^2}{\sin^2 \vartheta} \bar{P}_{nm}(\cos \vartheta)) \sin m\lambda \\
 \frac{\partial V_{xy}}{\partial \bar{S}_{nm}} = \frac{GMR^n}{r^{n+3}}(m \frac{1}{\sin \vartheta} \frac{\partial \bar{P}_{nm}(\cos \vartheta)}{\partial \vartheta} - m \frac{\cos \vartheta}{\sin^2 \vartheta} \bar{P}_{nm}(\cos \vartheta)) \cos m\lambda \\
 \frac{\partial V_{xz}}{\partial \bar{S}_{nm}} = \frac{GMR^n}{r^{n+3}}(n+2) \frac{\partial \bar{P}_{nm}(\cos \vartheta)}{\partial \vartheta} \sin m\lambda \\
 \frac{\partial V_{yz}}{\partial \bar{S}_{nm}} = \frac{GMR^n}{r^{n+3}} \frac{1}{\sin \vartheta} (m(n+2)\bar{P}_{nm}(\cos \vartheta)) \cos m\lambda
 \end{array} \right. \quad (9)$$

205 In next step, the linearization error is investigated using existing gravity
 206 field models along with GOCE track data which will be presented in Section
 207 4.

208 2.3 Determine the Weighting Formula

209 After linearization, which gives the observation matrix coefficients, the IGGT
 210 weighting formula is deduced by differentiating Eq.(2) to get Eq.(10):

$$\begin{aligned}
 dI = & -(V_{xx}dv_{xx} + V_{yy}dv_{yy} + V_{zz}dv_{zz}) \\
 & -2(V_{xy}dv_{xy} + V_{yz}dv_{yz} + V_{xz}dv_{xz})
 \end{aligned} \quad (10)$$

211 Using the adjusted law of measurement error propagation (Teunissen, 2000),
 212 the variance of the IGGT is given by Eq.(11):

$$D(I) = KD_{GGs}K^T = V_{xx}^2\sigma_{xx}^2 + V_{yy}^2\sigma_{yy}^2 + V_{zz}^2\sigma_{zz}^2 + 4V_{xy}^2\sigma_{xy}^2 + 4V_{yz}^2\sigma_{yz}^2 + 4V_{xz}^2\sigma_{xz}^2 \quad (11)$$

213 Since the V_{xy} and V_{yz} values for GOCE are degraded by a factor of 100 to
 214 1000 (Catastini et al, 2006), they are replaced in our study by synthetic values
 215 based on the a-priori model (c.f. section 3 for details). Therefore, the terms
 216 $4V_{yz}^2\sigma_{yz}^2$ and $4V_{xy}^2\sigma_{xy}^2$ in Eq.(11) are not included for the calculation of $D(I)$.
 217 Finally, Eq(12) gives the single weighting of the gravitational tensor invariant:

$$P_i = 1/D(I_i) \quad (12)$$

218 2.4 Regularization

219 Due to the problem of the polar gap in the GOCE data, the normal equa-
 220 tion matrix based on the GOCE GGs is ill-conditioned and must be regu-
 221 larized. We apply the SCRA as proposed by Metzler and Pail (2005) to the
 222 GOCE gravitational gradient normal equation from degree/order 2 to 150.
 223 Since the parameter vector x contains different coefficients than the a-priori
 224 model EIGEN-5C, we choose the stabilizing function $g_0=0$ (according to for-
 225 mula 27 in Metzler and Pail (2005)). Furthermore, for degree/order 150 and
 226 higher, Kaula's rule of thumb (Rapp, 1973; Reigber, 1989) is applied to the
 227 normal equation because for this degree range the low-order coefficients as well
 228 as all other short wavelength spherical harmonic coefficients are disturbed by
 229 the polar gap and the increasing sensitivity of the GOCE gradiometer. This
 230 can be seen in Figure 4(a). The optimal SCRA and Kaula rule parameters
 231 are empirically determined by comparing model-derived geoid heights with
 232 GNSS/Leveling data rather than with RMS geoid errors, as shown by Metzler
 233 and Pail (2005). We use this approach because the real gravity field, which
 234 is required to calculate the RMS geoid error, is unknown and this approach
 235 is best suited for simulations. The high accuracy of the GNSS/Leveling data
 236 and their wide distribution over several different countries and continents (see
 237 Table 2) make them best suitable for evaluation of our method.

238 3 Processing the Gravitational Gradients

239 3.1 Preprocessing

240 We use the components V_{xx}, V_{yy}, V_{zz} and V_{xz} of the GOCE GGs in the GRF
 241 taken from the Level2 product EGG_NOM.2 (ESA) which also contains the
 242 GRF to Inertial Reference Frame (IRF) attitude quaternions. For consistency
 243 with ESA's first generation gravity field models, we use data from November
 244 01, 2009 to January 11, 2010. Furthermore, we use the GOCE orbit position

245 given in the Earth-fixed Reference Frame (ERF) from the GOCE orbit prod-
 246 uct SST_PSO_2 which also includes the ERF to IRF quaternions. To deal
 247 with the two remaining but worse components of the GOCE GGs, a replace-
 248 ment strategy is used as described for the generation of ESA's GOCE product
 249 EGG_TRF_2 (Gruber et al, 2010). Here, the degraded components V_{xy} and
 250 V_{yz} of the GOCE GGs had been replaced by those computed from GOCE
 251 quick-look solution. But having in mind that the GOCE quick-look gravity
 252 field solutions are not computable satisfactory (Mayrhofer et al, 2010), we
 253 use reference GGs from the a-priori gravity field model EIGEN-5C to replace
 254 the worse components V_{xy} and V_{yz} . The reference U_{GRF} value for the GGs
 255 should first be calculated using EIGEN-5C in the LNOF (U_{LNOF}) and then
 256 transformed to the GRF (e.g. Fuchs and Bouman, 2011; Bouman et al, 2011):

$$U_{\text{GRF}} = (R_{\text{GRF}}^{\text{IRF}} R_{\text{IRF}}^{\text{ERF}} R_{\text{ERF}}^{\text{LNOF}}) U_{\text{LNOF}} (R_{\text{GRF}}^{\text{IRF}} R_{\text{IRF}}^{\text{ERF}} R_{\text{ERF}}^{\text{LNOF}})^T \quad (13)$$

257 where $R_{\text{GRF}}^{\text{IRF}}$ represents the transformation matrix to convert from the IRF
 258 to the GRF and $R_{\text{IRF}}^{\text{ERF}}$ is the transformation matrix to convert from ERF to
 259 IRF (which is taken from the quaternions in SST_PSO_2). The transformation
 260 matrix from LNOF to ERF is given by $R_{\text{ERF}}^{\text{LNOF}}$ and is taken from Eq.(14). Here,
 261 the latitude and longitude, λ and φ as well as the colatitude, $\vartheta = \pi/2 - \varphi$, can
 262 be calculated from the SST_PSO_2 orbit coordinates. The right side of U_{LNOF}
 263 in Eq.(13) is the transpose of $R_{\text{GRF}}^{\text{IRF}} R_{\text{IRF}}^{\text{ERF}} R_{\text{ERF}}^{\text{LNOF}}$.

$$R_{\text{ERF}}^{\text{LNOF}} = \begin{bmatrix} -\cos \lambda \cos \vartheta & \sin \lambda & \cos \lambda \sin \vartheta \\ -\sin \lambda \cos \vartheta & -\cos \lambda & \sin \lambda \sin \vartheta \\ \sin \vartheta & 0 & \cos \vartheta \end{bmatrix} \quad (14)$$

264 3.2 Filtering processing

265 After the reference GGs are calculated, the residuals of the used four GOCE
 266 gravity gradient components are obtained by subtracting the reference GGs
 267 from the measured GOCE GGs. These must then be filtered because the
 268 GOCE GGs are band-limited measurements. A forward and backward finite
 269 impulse response band-pass filter is used to account for the band-limited mea-
 270 surements according to Wan et al (2012). This approach can also eliminate
 271 phase change after filtering. As Figure 1 shows, the filter is of 1000th order
 272 with a band-pass frequency of 8.3-125 mHz. This band-pass frequency ensures
 273 that the results are as far as possible independent of the temporal variations in
 274 the colored noise (Bruinsma et al, 2014). The synthetic gravity gradient com-
 275 ponents V_{xy} and V_{yz} are not filtered and are taken as error-free observations.
 276 Figure 2 shows a power spectrum diagram of the filtering results; the Spectral
 277 Densities (SDs) for the gradient signal computed with the gravity field model
 278 are shown in red, the SDs for the GOCE gradient signal are shown in blue,
 279 and the difference in SDs between the gravity field model and the measured
 280 gradients, filtered to the band-pass frequency, are shown in green. The black
 281 line indicates the lower end of the specified band-pass frequency (8.3 mHz) and

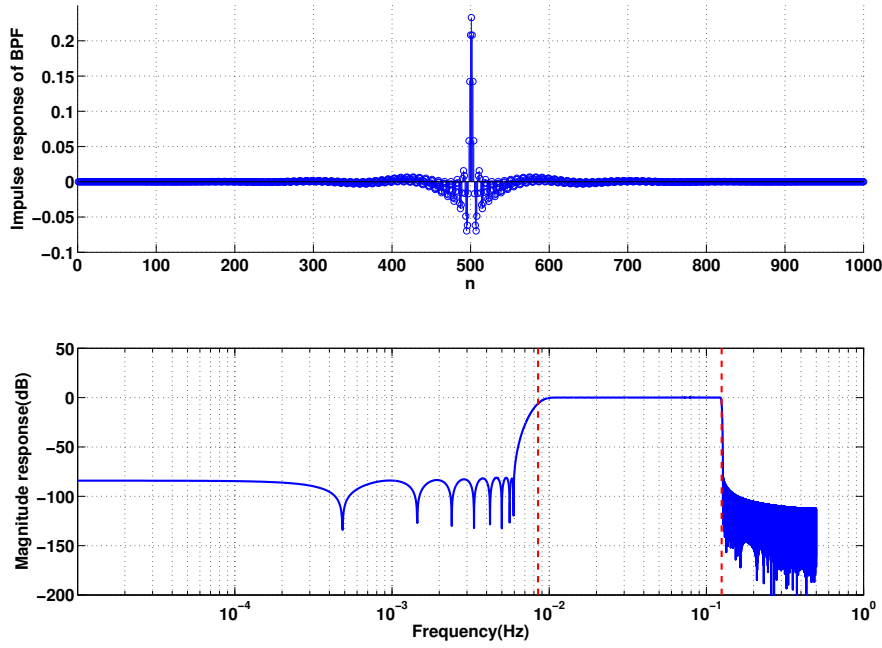


Fig. 1 Finite impulse response band-pass filter. The up half figure is the impulse response of the band-pass filter; The other half one is the magnitude response of the band-pass filter (unit: dB).

282 the cyan line indicates the upper end (125 mHz). The power spectrum of the
 283 signal in the filter band-pass remains almost the same, while the power spec-
 284 trum of the signal outside the pass-band is obviously decreased, representing a
 285 very small proportion of the total signal. This demonstrates the effectiveness
 286 of the filtering process. After filtering, we use the four accurate gravity gra-
 287 dient disturbance components, and their corresponding reference GGs, along
 288 with two other reference GGs to finally construct the gravitational gradient
 289 tensor as shown in Eq.(2).

290 4 Development of IGGT_R1

291 After determining the mathematic model and the stochastic model, we use
 292 GOCE GGs to build the gravity field model IGGT_R1. The main flowchart is
 293 shown in Figure 3: The input data and the filtering method are described in
 294 Section 3; The main methodology to use GOCE IGGT to build gravity field
 295 models by least squares method is mentioned in Section 2. The rest detailed
 296 informations of development of IGGT_R1 are given out as follow: EIGEN-5C
 297 is chosen as the a-priori gravity field model which is used to calculate $I(x_0)$ for
 298 linearization error analysis. As mentioned before, EGM2008 and EIGEN-6C4
 299 are used to calculate $I(x)$ to analyze the linearization error according to Eq. 6.

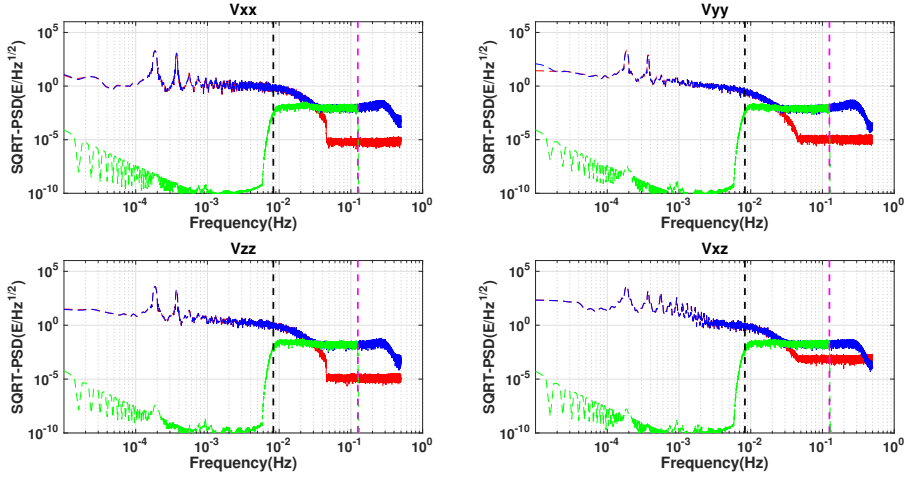


Fig. 2 Spectral densities for V_{xx} , V_{yy} , V_{zz} and V_{xz} for GRF (unit: E/\sqrt{Hz}). In red the Spectral Densities for the gradient signal computed with gravity field model, in blue the SDs for GOCE gradient signal, in green the SDs of the difference between gravity field model and measured gradients filtered to the band-pass frequency.

300 The positions are from one day's GOCE track data of 1 sec sampling rate and
 301 the maximum degree/order of the gravity field models is set to 240. The linear-
 302 ization error statistics are given in Table 1. Here, the Relative Linearization
 303 Error (RLE) is defined using Eq.(15):

$$\text{RLE} = \frac{1}{N} \sum_{i=1}^N \left| \frac{\text{Error}_{Li}}{I(x)_i} \right| \quad (15)$$

304 where N is the number of GOCE track data points. The relative linearization
 305 error is only about 0.00071% for the EGM2008 model and 0.00042% for the
 306 EIGEN-6C4 model. Using Eq.(10) and considering that the real accuracy of the
 307 GOCE GGs is of 2-4 mE (Bouman and Fuchs, 2012), the maximum absolute
 308 linearization error is approximately 10^{-21}s^{-4} and σ_I is $\sim 10^{-17}\text{-}10^{-16}\text{s}^{-4}$.
 This means the linearization error can be neglected in this study.

Table 1 Statistics of the Linearization Error of the a-priori gravity field model EIGEN-5C according to EGM2008 and the GOCE containing gravity field model EIGEN-6C4 as "true" models (Unit: s^{-4})

	EGM2008	EIGEN-6C4
Min	1.148699814359e-27	2.308982773258e-27
Max	2.167034978949e-21	7.978301266328e-22
Mean	2.090407160224e-23	1.497315373357e-23
STD	8.934785293679e-23	4.507380756543e-23
RLE	0.000711476171%	0.000423359387%

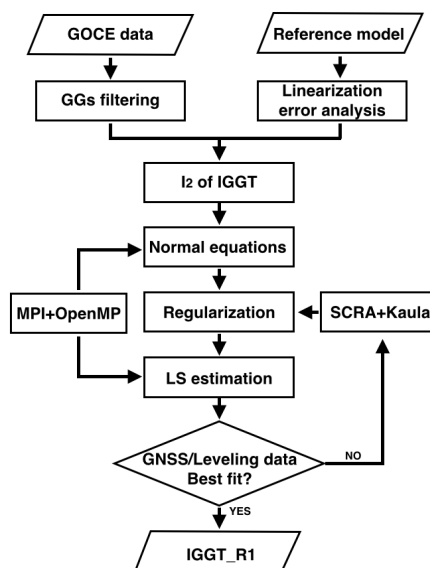


Fig. 3 Flowchart of the development of IGGT_R1. The LS estimation in the flowchart means least square estimation.

310 After studying the linearization error, one important step in the flowchart
 311 of the development of IGGT_R1 is about regularization which is already
 312 explained in Section 2.4. The results by compared with coefficients of EGM2008
 313 are shown in Figure 4: The SCRA and Kaula rule are effective by comparing
 314 these two sub-figures before and after regularization. It can be seen from the
 315 post regularization spectrum errors in Figure 4(b), the low-order coefficients
 316 and some short wavelength spherical harmonic coefficients are improved after
 regularization.

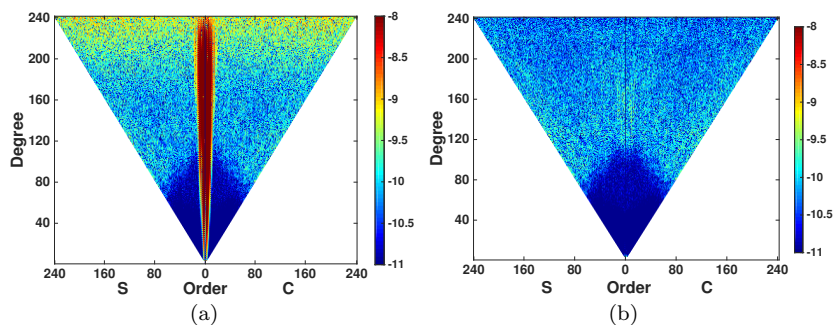


Fig. 4 Coefficient differences between IGGT_R1 and EGM2008 before regularization (a), after regularization (b), provided as absolute values in logarithmic scale (\log_{10}).

318 In the calculating process of building up gravity field models, especially
 319 dealing with a large number of satellite gravity measurement date sets by
 320 least square method, it needs to undertake large-scale numerical calculation.
 321 Aiming at this problem, we combine Message Passing Interface (MPI) and
 322 Open Multi-Processing (OpenMP) technology which also takes advantage of
 323 the symmetrical feature of normal equation matrix during the calculation. In
 324 this way, it can greatly accelerate the computation speed and improve the
 325 computational efficiency. The characteristic of MPI is processing level paral-
 326 lel granularity and memory data is distributed storage, so it can effectively
 327 decompose the program on different nodes at the same time to shorten run-
 328 ning time while the characteristic of OpenMP is thread level little granularity
 329 and memory data is shared storage, especially for calculating multiplication
 330 of small block matrix on the same node, so it can make full use of CPUs on
 331 single node to speed up the calculation process (e.g. Pacheco, 1997; Gropp
 332 et al, 1999; Chandra, 2001; Chapman et al, 2008).

333 5 Numerical results and analysis

334 To evaluate the spectral behavior we computed difference degree amplitudes
 335 for IGGT_R1 to EGM2008 and compared them to those for the gravity field
 336 models GO_CONS_GCF_2_TIM_R1 (TIM_R1), GO_CONS_GCF_2_SPW_R1 (SPW_R1),
 337 and GO_CONS_GCF_2_DIR_R2 (DIR_R2). TIM_R1 and SPW_R1 are part
 338 of ESA's first release of GOCE gravity field models (Pail et al, 2011) while
 339 DIR_R2 is part of ESA's second release of GOCE gravity field models (Bru-
 340 insma et al, 2010b). We compare IGGT_R1 with TIM_R1 and SPW_R1 as
 341 the data period for the GOCE GGs is the same. But we choose DIR_R2 in-
 342 stead of GO_CONS_GCF_2_DIR_R1 (DIR_R1) which belongs the ESA's first
 343 release of GOCE gravity field models since the high-degree parts of the model
 344 DIR_R1 are strongly constrained by regularization using a combined gravity
 345 field model containing terrestrial data (Pail et al, 2011). Figure 5 shows the
 346 obtained difference degree amplitudes. In the low-degree part (degree is less
 347 than 70), IGGT_R1 is closer to EGM2008 and consequently more accurate
 348 than TIM_R1, SPW_R1, and DIR_R2. This is because the SCRA is used for
 349 the low-degree part of IGGT_R1 and the GGs signal is replaced by the a-priori
 350 model EIGEN-5C outside the measurement bandwidth. It means that the low-
 351 degree part more closely matches the EIGEN-5C model (the blue line in the
 352 figure). From degree 75 to ~ 175 , IGGT_R1 is almost the same as TIM_R1,
 353 SPW_R1, and DIR_R2. This means that the contribution from the GOCE
 354 GGs to these gravity field models is basically the same at this degree range.
 355 In the high-end part (above degree 175), the difference degree amplitudes of
 356 IGGT_R1 are slightly lower than those of TIM_R1, SPW_R1 and DIR_R2. The
 357 main reason for this might be that the different regularization methods and
 358 parameters influence this part. When comparing IGGT_R1 with the a-priori
 359 model EIGEN-5C from degree 100 to 210, they are indistinguishable here,
 360 but the difference degree amplitudes of IGGT_R1 are slightly smaller than

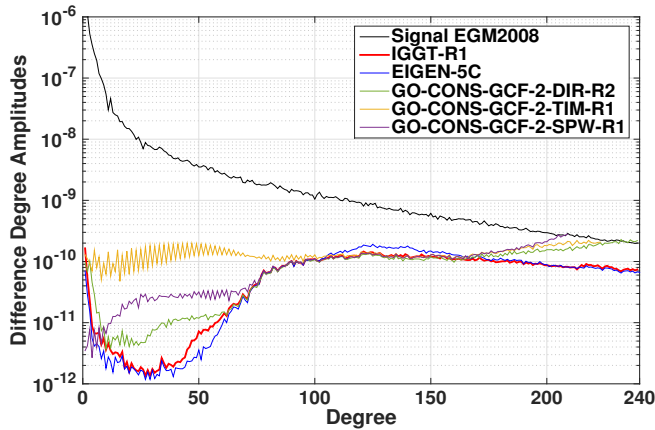


Fig. 5 Difference degree amplitudes (unitless) of several gravity field models w.r.t. EGM2008. The degree amplitudes of the EGM2008 model (black) are shown for reference.

361 those for EIGEN-5C. This means that IGGT_R1 might be more precise than
 362 EIGEN-5C in this region thanks to the GOCE GGs.

363 Figure 6 shows gravity anomaly differences between IGGT_R1 and EIGEN-
 364 5C. The large differences in Antarctica, South America, Africa, west China
 365 and Indonesia represent improvements due to the GOCE GGs. In other places
 366 like north America and Australia, EIGEN-5C already contains good ground
 367 gravimetry data. Figure 7 shows a histogram of the gravity anomaly differ-
 368 ences between IGGT_R1 and EIGEN-5C. The minimum, maximum, mean,
 369 and standard deviation of the gravity anomaly differences are -41.609, 49.791,
 370 -0.009, and 4.787 mGal, respectively.

371 In addition to our comparison with other global gravity field models, we
 372 check IGGT_R1 also using GNSS/Leveling data as independent data sets.
 373 Table 2 gives the RMS of the differences between GNSS/Leveling data and
 374 the model-derived geoid heights. In the first column of the table, SPW_R1,
 375 TIM_R1, DIR_R1, and DIR_R2 indicate the gravity field models mentioned
 376 before. From the table, the results of DIR_R1 are better than those of DIR_R2.
 377 This should be caused by the matter of fact that DIR_R1 has been regularized
 378 by using a combined gravity field model which contains terrestrial data. We
 379 also see that IGGT_R1 gives better results than SPW_R1 and TIM_R1. This
 380 should be caused by the impact of the a-priori model EIGEN-5C during the
 381 replacement procedure for the degraded components V_{xy} and V_{yz} of the GOCE
 382 GGs as mentioned above. That means IGGT_R1 has not only contributions
 383 from the GOCE GGs but contains also gravity field information from the a-
 384 prior gravity field model EIGEN-5C. Thus the results of the GNSS/Leveling
 385 check are relatively better. In comparison to DIR_R1 and DIR_R2, our model
 386 performs best in Germany and Japan with RMS values of 0.304 m and 0.545
 387 m. In other places, IGGT_R1, DIR_R1, and DIR_R2 have similar RMS values.
 388 By comparing with the a-priori gravity field model, the overall accuracy of

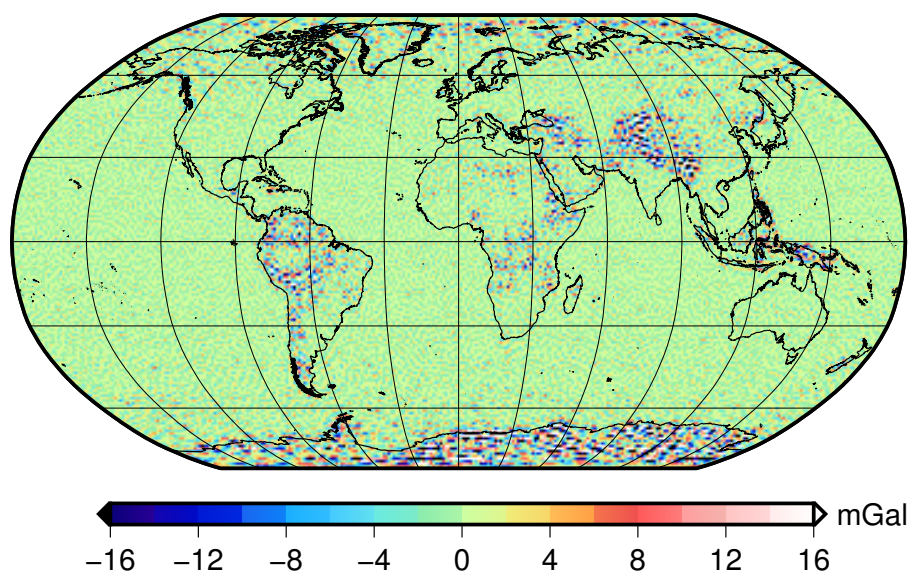


Fig. 6 Gravity anomaly differences (unit: mGal) between IGGT_R1 and EIGEN-5C at degree/order 240.

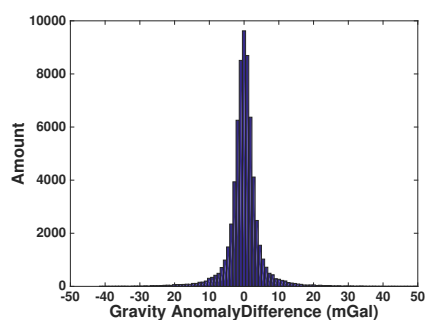


Fig. 7 Histogram of the gravity anomaly differences from Figure 6 (unit: mGal). Min/Max/Mean/STD are -41.609/49.791/-0.009/4.787 mGal.

389 IGGT_R1 is better or equal than EIGEN-5C. Specifically, the difference of the
 390 GNSS/Leveling performance between IGGT_R1 and EIGEN-5C is not very
 391 large for Germany, USA and Canada. The reason here may be that the a-priori
 392 gravity field model EIGEN-5C is already very accurate in these regions due to
 393 precise ground gravimetry data. The RMS difference between IGGT_R1's geoid
 394 heights and GNSS/Leveling data in Europe, Australia, Japan are improved by
 395 1.5 cm, 0.7 cm and 0.5 cm respectively due to the GOCE GGs. But for Brazil
 396 and China where EIGEN-5C has almost no contributions from terrestrial data
 397 we see a significant improvement by 6.7 cm and 4.1 cm due to the contribution
 398 of the GOCE GGs. It is also certified that the large gravity anomaly differences
 399 in South America and west China represent improvements due to the GOCE

Table 2 The RMS difference between GNSS/Leveling data (number of points in brackets) and model-derived geoid heights (unit: m). All models are taken to degree/order 210 which is the maximum degree of SPW_R1. IGGT_R1* is a gravity field model calculated as same as IGGT_R1 except that its a-priori model is EGM2008.

	Germany (675)	USA (6169)	Canada (1930)	Europe (1234)	Australia (201)	Japan (816)	Brazil (672)	China (990)
IGGT_R1	0.304	0.454	0.352	0.459	0.355	0.545	0.434	0.582
EIGEN-5C	0.303	0.456	0.353	0.474	0.362	0.550	0.501	0.623
IGGT_R1*	0.309	0.448	0.350	0.453	0.350	0.542	0.421	0.549
EGM2008	0.306	0.447	0.344	0.455	0.356	0.536	0.457	0.579
EIGEN-6S4v2	0.308	0.447	0.345	0.452	0.355	0.542	0.419	0.540
SPW_R1	0.331	0.470	0.399	0.495	0.383	0.569	0.447	0.589
TIM_R1	0.337	0.460	0.376	0.485	0.379	0.575	0.433	0.577
DIR_R1	0.308	0.446	0.349	0.458	0.354	0.546	0.417	0.552
DIR_R2	0.322	0.450	0.356	0.456	0.370	0.555	0.422	0.572

Sources/References for the used GNSS/Leveling data:

USA: Milbert (1998)

Canada: M. Vronneau, personal communication 2003, Natural Resources Canada

Europe/Germany: Ihde et al (2002)

Australia: G. Johnston, Geoscience Australia and W. Featherstone, Curtin University of Technology, personal communication 2007

Japan: Tokuro Kodama, Geospatial Information Authority of Japan, personal communication (2013)

Brazil: Denizar Blitzkow and Ana Cristina Oliveira Cancoro de Matos, Centro de Estudos de Geodesia (CENEGEO), personal communication, the data belongs to the Brazilian Institute of Geography and Statistics (IBGE)

China: National GNSS Leveling A/B: Zhang et al (2009) and Li et al (2014)

400 GGs as mentioned before. Furthermore, to examine the influence of different
 401 a-priori gravity field models to the approach in this paper, we also choose
 402 EGM2008 as the a-priori gravity field model to build a gravity field model
 403 named IGGT_R1*. The GNSS/Leveling checking results are also shown in
 404 Table 2: IGGT_R1* is better than IGGT_R1 and reaches the accuracy of the
 405 latest satellite-only gravity field model EIGEN-6S4v2 (Förste et al, 2015b);
 406 The overall improvement of IGGT_R1* to EGM2008 is in Brazil and China
 407 by 3.6 cm and 3.0 cm. The reason here may be that the accuracy of EGM2008
 408 is higher than EIGEN-5C and is already very good at some places where exist
 409 precise terrestrial data. But GOCE GGs have contributions in the other places.

410

411 Finally, we apply an oceanographic evaluation on IGGT_R1. Figure 8
 412 shows the geostrophic velocity speed in the Agulhas current area at a res-
 413 olution of about 27 km. Geostrophic velocity speed is derived from the ocean's
 414 Mean Dynamic Topography (MDT), as described by Knudsen and Benveniste
 415 (2011); Knudsen et al (2011). A remove-restore technique is used to com-
 416 pute the combined MDT, which contains both the low-frequency signal of
 417 satellite-only MDT and the high-frequency signal from the a priori MDT
 418 (MDT_DTU_10.2M.nc). MDT_DTU_10.2M.nc is produced by the Danish Na-
 419 tional Space Center and it includes TOPEX Ellipsoid and Mean-Tide system

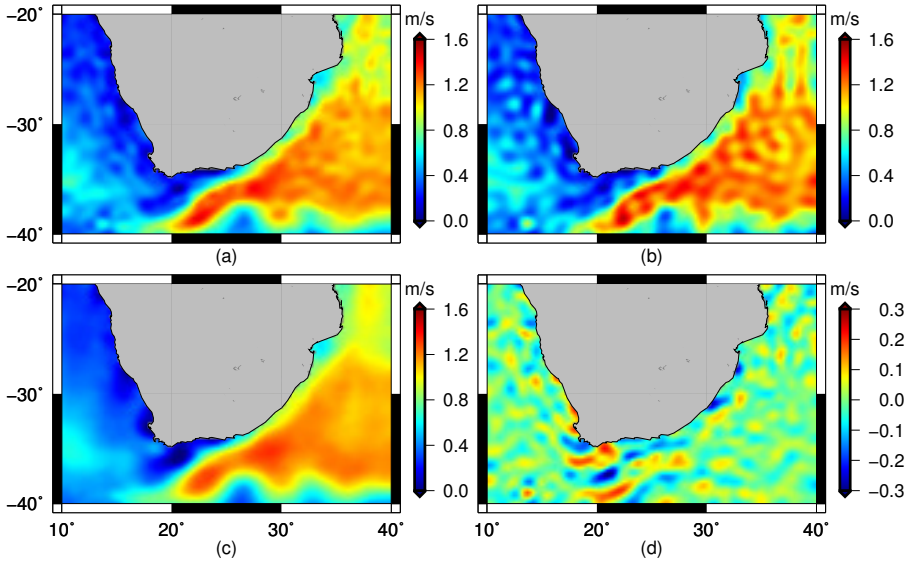


Fig. 8 Geostrophic velocity speed (unit: m s^{-1}) in the Agulhas current area at a resolution of about 27 km from (a) IGGT_R1, (b) TIM_R1, and (c) EIGEN-5C. Panel (d) shows the difference in geostrophic velocity speed between IGGT_R1 and EIGEN-5C.

420 metadata. As can be seen from the figure 8, the geostrophic velocity speed
 421 from IGGT_R1 is not as smooth as that from EIGEN-5C. Panel d of Figure 8
 422 shows the difference between these two models. The minimum, maximum,
 423 mean, and RMS of the difference between the models are -0.310, 0.219, -0.0068,
 424 and 0.0589 m s^{-1} , respectively. These differences might be due to the GOCE
 425 GGs, but this cannot be confirmed without real drifter velocity measurements.
 426 The geostrophic velocity speed from TIM_R1 is a little more discrepant with
 427 EIGEN-5C. The main reason for this might be that the low-degree coefficients
 428 of TIM_R1 are not very accurate, as shown in Figure 5.

429 6 Discussion and Conclusions

430 The gravity field model IGGT_R1 has been generated using the GOCE IGGT
 431 by least squares method as described in this article. Due to the special char-
 432 acteristics of IGGT, this model avoids errors introduced by inaccurate mea-
 433 surement of the satellite's attitude during the traditional coordinate transfor-
 434 mations. Additionally, according to the principle of least squares, the direct
 435 solution method is theoretically strict and there are no grid or integral dis-
 436 cretization errors introduced in the harmonic analysis. The linearization error
 437 can be neglected if the a-priori gravity field model is relatively accurate. In
 438 such a case the corresponding linearization error is smaller than the accuracy
 439 of the GOCE GGs. Using the SCRA in combination with the Kaula rule is an
 440 effective way to solve the ill-conditioned problem of the normal equation which

441 primarily helps to improve the low-order coefficients. From numerical analy-
442 ses, we show that the precision of the obtained gravity anomaly values over
443 Antarctica, South America, Africa, west China and Indonesia are improved
444 due to the GOCE GGs. The RMS difference between GNSS/Leveling data
445 and the model-derived geoid heights shows that IGGT_R1 is more precise than
446 SPW_R1 and TIM_R1, and it performs similarly to DIR_R1 and DIR_R2. In
447 comparison to the a-priori gravity field model EIGEN-5C, the whole accuracy
448 of IGGT_R1 is improved according to the GNSS/Leveling checking results.
449 This represents the contribution of the GOCE GGs, especially in Brazil and
450 China. According to geostrophic velocity speeds in the Agulhas current area,
451 IGGT_R1, which yields more details because of the GOCE GGs, might be an
452 improvement over EIGEN-5C. Considering time-consuming of calculation by
453 the least squares method, IGGT_R1 contains the same GOCE GGs as ESA's
454 first released gravity field models. In the future, all the GGs data of GOCE
455 mission may be contained to calculate a more precise gravity field model. Our
456 conclusion is that high precision gravity field models can be obtained using the
457 approach as outlined in this paper. This provides a new direction for building
458 gravity field models from the GOCE GGs as well as from future satellite GGs.

459 **Acknowledgements** Thanks for the constructive comments and beneficial suggestions
460 from the anonymous reviewers and editors, which help us a lot for improving this manuscript.
461 We also would like to express appreciation to Dr. X.Y. Wan of Qian Xuesen Laboratory
462 of Space Technology (QLST), Dr. O. Abrykosov of German Research Centre for Geo-
463 sciences (GFZ) and Dr. J. Bouman of German Geodetic Research Institute (DGFI) for their
464 kind help and discussions. This study is supported by the Chinese Scholarship Council
465 (No. 201506270158), the Natural Science Foundation of China (No. 41131067, 41374023,
466 41474019) and the Key Laboratory of Geospace Environment and Geodesy, Ministry Edu-
467 cation, Wuhan University (No. 16-02-07).

468 References

- 469 Barthelmes F (2009) Calculation Service ICGEM [http://icgem.gfz-potsdam.](http://icgem.gfz-potsdam.de)
470 [de](http://icgem.gfz-potsdam.de)
- 471 Barthelmes F, Förste C (2011) The ICGEM-format. Potsdam: GFZ German
472 Research Centre for Geosciences, Department 1
- 473 Baur O, Sneeuw N, Grafarend EW (2008) Methodology and use of tensor
474 invariants for satellite gravity gradiometry. *Journal of Geodesy* 82(4-5):279–
475 293
- 476 Bouman J, Fuchs MJ (2012) GOCE gravity gradients versus global gravity
477 field models. *Geophysical Journal International* 189(2):846–850
- 478 Bouman J, Fiorot S, Fuchs M, Gruber T, Schrama E, Tscherning C, Veicherts
479 M, Visser P (2011) GOCE gravitational gradients along the orbit. *Journal*
480 *of Geodesy* 85(11):791–805
- 481 Bruinsma S, Marty J, Balmino G, Biancale R, Foerste C, Abrikosov O, Neu-
482 mayer H (2010a) GOCE gravity field recovery by means of the direct numerical
483 method, paper presented at the ESA Living Planet Symposium, Eur.
484 Space Agency, Bergen Norway, June pp 28–2

- 485 Bruinsma SL, Förste C, Abrikosov O, Lemoine JM, Marty JC (2010b) ESAs
486 GOCE gravity field model from the Direct Approach release 2. available
487 from the ICGEM data base at GFZ Potsdam, <http://icgemgfz-potsdam.de>
488 Bruinsma SL, Förste C, Abrikosov O, Lemoine JM, Marty JC, Mulet S, Rio
489 MH, Bonvalot S (2014) ESA's satellite-only gravity field model via the
490 direct approach based on all GOCE data. *Geophysical Research Letters*
491 41(21):7508–7514
- 492 Catastini G, Cesare S, De Sanctis S, Dumontel M, Parisch M, Sechi G (2006)
493 Predictions of the GOCE in-flight performances with the end-to-end system
494 simulator. In: *Proceedings of the 3rd international GOCE user workshop*,
495 pp 6–8
- 496 Chandra R (2001) *Parallel programming in OpenMP*. Morgan kaufmann
- 497 Chapman B, Jost G, Van Der Pas R (2008) *Using OpenMP: portable shared
498 memory parallel programming*, vol 10. MIT press
- 499 Colombo OL (1981) *Numerical methods for harmonic analysis on the sphere*.
500 Tech. rep., DTIC Document
- 501 Courant R, John F (2012) *Introduction to calculus and analysis*, vol 1. Springer
502 Science & Business Media
- 503 Förste C, Flechtner F, Schmidt R, Stubenvoll R, Rothacher M, Kusche J,
504 Neumayer KH, Biancale R, Lemoine JM, Barthelmes F, Bruinsma J, König
505 R, Meyer U (2008) EIGEN-GL05C-A new global combined high-resolution
506 GRACE-based gravity field model of the GFZ-GRGS cooperation. In: *Geo-
507 physical Research Abstracts*, vol 10, pp EGU2008–A
- 508 Förste C, Bruinsma S, Abrikosov O, Lemoine J, Marty J, Flechtner F,
509 Balmino G, Barthelmes F, Biancale RE (2015a) EIGEN-6C4 The latest
510 combined global gravity field model including GOCE data up to degree
511 and order 2190 of GFZ Potsdam and GRGS Toulouse. GFZ Data Services
512 <http://doi.org/105880/icgem20151>
- 513 Förste C, Bruinsma S, Rudenko S, Abrikosov O, Lemoine JM, Marty JC,
514 Neumayer H, Biancale R (2015b) EIGEN-6S4: A time-variable satellite-
515 only gravity field model to d/o 300 based on LAGEOS, GRACE and GOCE
516 data from the collaboration of GFZ Potsdam and GRGS Toulouse. In: *EGU
517 General Assembly Conference Abstracts*, vol 17, p 3608
- 518 Fuchs MJ, Bouman J (2011) Rotation of GOCE gravity gradients to local
519 frames. *Geophysical Journal International* 187(2):743–753
- 520 Gropp W, Lusk E, Skjellum A (1999) *Using MPI: portable parallel program-
521 ming with the message-passing interface*, vol 1. MIT press
- 522 Gruber T, Rummel R, Abrikosov O, van Hees R (2010) *GOCE level 2 product
523 data handbook*. Tech. rep., GO-MA-HPF-GS-0110
- 524 Heiskanen WA, Moritz H (1967) *Physical geodesy*. *Bulletin Géodésique* (1946-
525 1975) 86(1):491–492
- 526 Holota P (1989) Boundary value problems and invariants of the gravitational
527 tensor in satellite gradiometry. In: *Theory of Satellite Geodesy and Gravity
528 Field Determination*, Springer, pp 447–457
- 529 Ihde J, Adam J, Gurtner W, Harsson B, Sacher M, Schlüter W, Wöppelmann
530 G (2002) The Height Solution of the European Vertical Reference Network

- 531 (EUVN), Mitteilungen des BKG, Bd. 25, EUREF Publication No. 11/I,
532 Frankfurt a. M, Germany pp 53–79
- 533 Klees R, Koop R, Visser P, Van den Ijssel J (2000) Efficient gravity field
534 recovery from GOCE gravity gradient observations. *Journal of geodesy* 74(7-
535 8):561–571
- 536 Knudsen P, Benveniste J (2011) GOCE user toolbox and tutorial. In: Pro-
537 ceedings of the 4th International GOCE User Workshop, European Space
538 Agency, ESA Publication SP-696, 4p Munich
- 539 Knudsen P, Bingham R, Andersen O, Rio MH (2011) A global mean dynamic
540 topography and ocean circulation estimation using a preliminary GOCE
541 gravity model. *Journal of Geodesy* 85(11):861–879
- 542 Koop R (1993) Global gravity field modeling using satellite gravity gradiom-
543 etry. *Publications on Geodesy*, 38
- 544 Li J, Jiang W, Zou X, Xu X, Shen W (2014) Evaluation of recent GRACE and
545 GOCE satellite gravity models and combined models using GPS/leveling
546 and gravity data in china. In: *Gravity, Geoid and Height Systems*, Springer,
547 pp 67–74
- 548 Mayrhofer R, Pail R, Fecher T (2010) Quick-look gravity field solution as part
549 of the GOCE quality assessment. In: *Proceedings of the ESA Living Planet*
550 *Symposium*, vol 28
- 551 Metzler B, Pail R (2005) GOCE data processing: the spherical cap regulariza-
552 tion approach. *Studia Geophysica et Geodaetica* 49(4):441–462
- 553 Migliaccio F, Reguzzoni M, Sansò F (2004) Space-wise approach to satellite
554 gravity field determination in the presence of coloured noise. *Journal of*
555 *Geodesy* 78(4-5):304–313
- 556 Migliaccio F, Reguzzoni M, Gatti A, Sansò F, Herceg M (2011) A GOCE-only
557 global gravity field model by the space-wise approach. In: *4th International*
558 *GOCE User Workshop*
- 559 Milbert DG (1998) Documentation for the GPS benchmark data set of 23-
560 july-98. *IGeS Bulletin* (8):29–42
- 561 Pacheco PS (1997) *Parallel programming with MPI*. Morgan Kaufmann
- 562 Pail R, Plank G (2002) Assessment of three numerical solution strategies for
563 gravity field recovery from GOCE satellite gravity gradiometry implemented
564 on a parallel platform. *Journal of Geodesy* 76(8):462–474
- 565 Pail R, Schuh WD, Wermuth M (2005) GOCE gravity field processing. In:
566 *Gravity, Geoid and Space Missions*, Springer, pp 36–41
- 567 Pail R, Bruinsma S, Migliaccio F, Förste C, Goiginger H, Schuh WD, Höck E,
568 Reguzzoni M, Brockmann JM, Abrikosov O, Martin V, Thomas F, Reinhard
569 M, Ina K, Fernando S, Carl CT (2011) First GOCE gravity field models
570 derived by three different approaches. *Journal of Geodesy* 85(11):819–843
- 571 Pavlis NK, Holmes SA, Kenyon SC, Factor JK (2012) The development and
572 evaluation of the Earth Gravitational Model 2008 (EGM2008). *Journal of*
573 *Geophysical Research: Solid Earth* 117(B4)
- 574 Rapp RH (1973) Improved models for potential coefficients and anomaly de-
575 gree variances. *Journal of Geophysical Research* 78(17):3497–3500

- 576 Reguzzoni M, Tselmes N (2009) Optimal multi-step collocation: application
577 to the space-wise approach for GOCE data analysis. *Journal of Geodesy*
578 83(1):13–29
- 579 Reigber C (1989) Gravity field recovery from satellite tracking data. In: *Theory*
580 *of satellite geodesy and gravity field determination*, Springer, pp 197–234
- 581 Rummel R (1993) On the Principles and Prospects of Gravity Field Determination
582 by Satellite Methods. In: *Geodesy and Physics of the Earth*, Springer,
583 pp 67–70
- 584 Rummel R, Colombo O (1985) Gravity field determination from satellite gradiometry.
585 *Bulletin géodésique* 59(3):233–246
- 586 Rummel R, Yi W, Stummer C (2011) GOCE gravitational gradiometry. *Journal*
587 *of Geodesy* 85(11):777–790
- 588 Sacerdote F, Sansò F (1989) Some problems related to satellite gradiometry.
589 *Bulletin géodésique* 63(4):405–415
- 590 Schuh WD (1996) Tailored numerical solution strategies for the global determination
591 of the Earth’s gravity field. *Mitteilungen der geodtischen Institute*
592 *der Technischen Universitt Graz*, Folge 81, Graz 1996
- 593 Schuh WD (2003) The processing of band-limited measurements; filtering techniques
594 in the least squares context and in the presence of data gaps. In: *Earth Gravity Field from Space*
595 *From Sensors to Earth Sciences*, Springer, pp 67–78
- 596 Taylor B (1717) *Methodus incrementorum directa & inversa*. Inny
- 597 Teunissen PJ (2000) *Adjustment theory: an introduction*. Delft University
598 Press Delft
- 599 Vermeer M (1990) Observable quantities in satellite gradiometry. *Bulletin*
600 *géodésique* 64(4):347–361
- 601 Wan XY, Yu JH, Zeng YY (2012) Frequency Analysis and Filtering Processing of Gravity
602 Gradient Data from GOCE. *Chinese Journal of Geophysics*
603 55(5):530–538
- 604 Yi W (2012) An alternative computation of a gravity field model from GOCE.
605 *Advances in Space Research* 50(3):371–384
- 606 Yu J, Wan X (2013) Recovery of the gravity field from GOCE data by using the
607 invariants of gradient tensor. *Science China Earth Sciences* 56(7):1193–1199
- 608 Yu J, Zhao D (2010) The gravitational gradient tensors invariants and the
609 related boundary conditions. *Science China Earth Sciences* 53(5):781–790
- 610 Zhang C, Guo C, Chen J, Zhang L, Wang B (2009) EGM2008 and Its Application
611 Analysis in Chinese Mainland. *Acta Geodaetica et Cartographica Sinica*
612 38(4):283–289
- 613